Deformable Medical Image Registration: Setting the State of the Art with Discrete Methods*

Ben Glocker,[1,4,**] Aristeidis Sotiras,[2,**] Nikos Komodakis,[3] and Nikos Paragios[2]

[1]Computer Aided Medical Procedures, Technische Universität München, 85748 Garching, Germany

[2]Department of Applied Mathematics, École Centrale de Paris/INRIA Saclay, Ile-de-France, 92290 Orsay, France; email: nikos.paragios@ecp.fr

[3]Computer Science Department, University of Crete, Heraklion, Greece

[4]Current address: Microsoft Research Cambridge, United Kingdom

Annu. Rev. Biomed. Eng. 2011. 13:219–44

First published online as a Review in Advance on May 9, 2011

The *Annual Review of Biomedical Engineering* is online at bioeng.annualreviews.org

This article's doi: 10.1146/annurev-bioeng-071910-124649

1523-9829/11/0815-0219$20.00

*The proposed registration framework, along with a graphical interface and corresponding publications, is available for download for research purposes (for Windows and Linux platforms) from **http://www.mrf-registration.net**.

**These authors contributed equally to this work.

Keywords

Markov random fields, geometric registration, iconic registration, discrete labeling, linear programming

Abstract

This review introduces a novel deformable image registration paradigm that exploits Markov random field formulation and powerful discrete optimization algorithms. We express deformable registration as a minimal cost graph problem, where nodes correspond to the deformation grid, a node's connectivity corresponds to regularization constraints, and labels correspond to 3D deformations. To cope with both iconic and geometric (landmark-based) registration, we introduce two graphical models, one for each subproblem. The two graphs share interconnected variables, leading to a modular, powerful, and flexible formulation that can account for arbitrary image-matching criteria, various local deformation models, and regularization constraints. To cope with the corresponding optimization problem, we adopt two optimization strategies: a computationally efficient one and a tight relaxation alternative. Promising results demonstrate the potential of this approach. Discrete methods are an important new trend in medical image registration, as they provide several improvements over the more traditional continuous methods. This is illustrated with several key examples where the presented framework outperforms existing general-purpose registration methods in terms of both performance and computational complexity. Our methods become of particular interest in applications where computation time is a critical issue, as in intraoperative imaging, or where the huge variation in data demands complex and application-specific matching criteria, as in large-scale multimodal population studies.

Contents

1. INTRODUCTION

Image registration involves determining a spatial transformation that establishes meaningful correspondences between a set of images. This is a predominant task in biomedical imaging with applications to population modeling, longitudinal studies, and computer-assisted diagnosis and interventions.

The number of clinical examples involving dense registration/fusion is phenomenal. For demonstration purposes, we provide some examples relating to the problem of image registration discussed in this review. First, one can cite spatiotemporal acquisitions of deformable organs involving motion, such as strain estimation from (tagged) magnetic resonance (MR) (1) where deformable fusion becomes equivalent to motion estimation. Addressing the same problem can become even more challenging when the image intensities change over time under the influence of a contrast agent, as in the case of dynamic contrast-enhanced images for prostate tumor cancer detection (2). Deformable fusion of static organs aims to find functional and anatomical correspondences, as in the case of positron emission tomography–computed tomography (PET-CT) (3), and it has applications to numerous clinical examples. Longitudinal organ modeling and the study of disease progression is another example where registration plays a key role. One can cite tumor evolution prediction methods with applications to brain imaging (4, 5); the aim of registration in that case is to determine a measure of progression for the tumor. Furthermore, most of the functional studies involving functional magnetic resonance imaging (fMRI) have a prerequisite deformable registration (6) toward a common reference (often the Talairach space). Such a step is necessary toward functional understanding of the brain between normal and diseased subjects [e.g., see numerous Alzheimer studies (7–9)]. Fusion between preoperative and interventional images is another great example where registration is a vital element of the process. Radiotherapy (10) targets tumorous cells based on high-resolution CT data. Failure to account for the displacement of the subject during treatment eventually may lead to destruction of healthy cells. Brain surgery is

another example where deformable fusion is critical owing to the problem of brain matter collapse after the scalp is opened (11). The use of registration between preoperative and interventional data could lead to precise delineation of the tumor and therefore could increase the chances of recovery after surgery with a reduced number of side effects.

FFD: free-form deformation

Image registration involves three main aspects: (*a*) the adoption of an image transformation model, (*b*) the definition of an objective function based on an image-matching criterion, and (*c*) the employment of an optimization strategy that estimates the optimal transformation parameters with respect to the objective function. The field of image registration has been studied for more than three decades, and the many image registration methods differ mainly in the particular choices made for the three main aspects. A complete overview is beyond the scope of this review, so we would like to point the reader to the books by Hajnal et al. (12) and Modersitzki (13), the surveys by Maintz & Viergever (14) and Zitova & Flusser (15), and the tutorial by Szeliski (16). In the following, we briefly introduce the basic principles and components common in many algorithms and discuss some popular choices and models.

Image transformations can be either linear or nonlinear. Rigid and affine transformations are the most common examples of linear parametric models used for image registration. Such global models offer a compromise between (*a*) low computational complexity and high robustness of the estimation and (*b*) low accuracy in terms of local matching. These models are often used in longitudinal studies where the assumption of global alignment (as with bones, for example) is valid because the same subject is imaged. Nonlinear transformations representing deformations are a more precise way to cope with the variability of the human anatomy, as well as with nonrigid motions of deformable anatomical structures such as soft tissue. Several compact and highly efficient transformation models have been introduced in medical imaging for nonrigid alignment, such as free-form deformations (FFDs) (17), thin-plate splines (18), radial basis functions (19), or finite elements (20), all of which offer a compromise between computational complexity and deformation abilities. More recently, the idea of piece-wise linear transformations was introduced (21); through these types of transformations, one seeks to determine alignment through accumulation of local linear models.

The definition of the registration objective function, and in particular the matching criterion, is more challenging, at least when referring to the multimodal case where images from different sources need to be registered. This mostly arises from the different physical principles behind the acquisition processes. In general, registration can be solved in different ways, each of which affects the definition of the objective function. We can roughly separate registration methods into two main categories: geometric registration and iconic registration.

Geometric registration is based on finding correspondences between meaningful anatomical locations or salient landmarks (22), which first need to be extracted from the images. The optimization process seeks a transformation that optimally maps corresponding landmarks to each other (18, 23–25). Here, the matching criterion could be simply defined, for instance, as the (Euclidean) distance between the point sets where the optimal transformation is found when the distance is minimal. The extraction of landmarks is often nontrivial and might involve a challenging process; at the same time, the support of the landmarks is often sparse regarding the overall deformation. Therefore, interpolation strategies such as thin-plate splines (26) are considered in order to determine a dense registration for all image points.

Iconic methods involve using image intensities directly to perform registration. The matching criterion then comes from an intensity-based similarity measure that evaluates how "similar" the images are with respect to their appearance and the transformation. For instance, in intramodal scenarios where the images are acquired with the same device and a similar intensity distribution can be assumed, a similarity measure based on the (normalized) sum of absolute differences or cross

correlation can be sufficient (12). The optimal transformation is then found by minimizing the intensity differences or maximizing the correlation between the images. In the case of intermodal registration, this is more complex, and researchers have focused on the development of universal measures based on statistical principles that can determine the similarity of images acquired with different sensors. Examples are correlation ratio (27), mutual information (MI) (28, 29), and Kullback-Leibler divergence (30). These measures perform well when their underlying statistical assumptions are satisfied from the acquisitions (which often is not the case for a general multimodal registration problem).

MI: mutual information

MRF: Markov random field

LP: linear programming

More recently, owing to progress made in the machine-learning community, methods targeting either landmark extraction and selection as well as optimal feature selection (mutual saliency, for example) or direct metric learning were considered (31, 32). The underlying idea is to map one set of observations to another using a linear or nonlinear mapping learned from training examples (33).

Our focus in this review is on deformable registration. Once the nonlinear transformation model and a suitable objective function have been defined, the last task consists of finding the optimal set of parameters. Such an optimization process is challenging in terms of both computational and qualitative performance. This arises from the fact that nonlinear registration is often ill-posed (this applies in particular to iconic registration because the number of constraints are inferior to the number of parameters to be estimated), nonlinear (because the transformation parameters are related to the observations in the most general case in a nonlinear manner), and nonconvex (due to the dimensionality of the search space as well as the nature of the functions being considered).

Both continuous (34) and discrete (35, 36) optimization methods often are considered for the third aspect of parameter estimation, where a trade-off between precision versus computational load is to be found. Continuous methods do not inherit any constraints on the nature of the objective function; the drawback is that these methods are sensitive to the initial conditions, nonmodular with respect to the objective function and to the nature of transformation, and often computationally inefficient. Conversely, discrete methods are less sensitive to the initial conditions and often converge faster compared with the continuous methods; at the same time, the discrete methods are constrained by limited precision owing to the quantization of the solution space.

In this review, we present a universal formulation to cope with deformable image registration. It is based on the concept of Markov random fields (MRFs) and discrete optimization. Registration is expressed as an iterative labeling problem of a graph. Nodes of the graph correspond to deformation elements that can be either image points or less complex graph models associated with a compact model and an interpolation strategy. Connections on the graph denote dependencies between single deformations of correlated nodes (neighboring nodes constitute the simplest case). The graph is associated with a set of labels, each of which corresponds to an update on the deformation. Node-labeling costs are determined either by measuring geometric consistency between extracted landmarks or by evaluating an intensity-based similarity measure on local image patches undergoing deformations. The introduction of additional costs for the consistency of correlated nodes favors smooth deformations. Such a framework can cope with arbitrary geometric and iconic matching criteria and deformation models (preferably with low connectivity) while providing strong solutions at a fast convergence rate. We consider recent advances in the area of discrete optimization, and, depending on the complexity of the graph structure, we explore linear programming (LP) and message passing for recovering the optimal transformation parameters.

The remainder of this review is organized as follows. In Section 2, we present a general framework for geometric, iconic, hybrid, and coupled image registration in continuous domains. We then present the decomposition of the corresponding objective functions toward a mapping into a

discrete graph structure. In Section 3, we introduce the concept of discrete labeling in MRFs and how this can be used for solving deformable registration. Section 3.3 is dedicated to the optimization of the designed MRF energy function. Implementation details and experimental validation are discussed in Section 4, and Section 5 offers a conclusion.

2. DEFORMABLE IMAGE REGISTRATION

We focus on the case of pairwise registration of two d-dimensional intensity images $I, J : \Omega \subset \mathbb{R}^d \mapsto \mathbb{R}$, where one of the images, let us say I, is undergoing a transformation denoted by $I \circ T$, with $T : \mathbb{R}^d \mapsto \mathbb{R}^d$ being a spatial mapping. The transformed image is also termed the source image or moving image. The image J remains fixed and is termed the target or reference image. We consider the case of nonlinear or deformable registration where the transformation is defined in the most general case as the addition of the identity mapping and a dense displacement field D:

$$T(x) = x + D(x), \tag{1}$$

where $x \in \Omega$ is a point in the image domain and $D(x)$ is a d-dimensional displacement vector. The task of the registration algorithm is then to estimate the optimal displacement field given the images. This is commonly formulated as an optimization problem of the form

$$\hat{T} = \arg\min_{T} \mathcal{E}(T), \tag{2}$$

where $\hat{T}$ is the optimal transformation at the minimum of the objective function $\mathcal{E}$ (also known as the energy function). This function consists of a matching criterion $\mathcal{M}$ and an additional regularization term $\mathcal{R}$, which renders the problem well posed. The objective function is then defined as $\mathcal{E} = \mathcal{M} + \mathcal{R}$.

Throughout this review, we assume a minimization problem with respect to $\mathcal{E}$, even if it involves a matching criterion that originally would need to be maximized. However, every function can be transformed easily such that it can be minimized equivalently. From a Bayesian perspective, minimizing the above energy is equivalent to maximizing the posterior distribution $p(T|I, J) \propto p(I, J|T)p(T)$, where the likelihood $p(I, J|T)$ corresponds to our (data-dependent) matching criterion $\mathcal{M}$ and the regularization term $\mathcal{R}$ plays the role of the prior $p(T)$.

Let us now discuss the details for the two terms $\mathcal{M}$ and $\mathcal{R}$. In general, the registration can be done in different ways, and most algorithms belong either to the geometric class of methods or to the iconic class of methods. Depending on the class, different types of matching criteria are defined. Geometric methods aim to determine optimal correspondences between meaningful anatomical landmarks, whereas iconic methods seek to optimize the "visual" correspondences in terms of image intensities. Let us start with a discussion on geometric registration.

2.1. Geometric Registration

Assume we have extracted two sets of landmarks, $K = \{\kappa_1, \ldots, \kappa_n\} \in \Omega_I$ and $\Lambda = \{\lambda_1, \ldots, \lambda_m\} \in \Omega_J$, from the two images I and J. Key examples of geometric registration might be its use for matching points sampled from two surfaces such as in image-guided brain surgery (37–39) or its use for marker-based registration in cardiac motion validation problems (40, 41). How we can extract such landmarks is discussed in Section 4, Experimental Validation. In general, the two sets do not necessarily need to have the same cardinality (i.e., $n \neq m$), and we do not know in advance which landmarks correspond to each other. However, we suppose that in these two sets, the points that correspond to the true underlying anatomical correspondence are contained. In the next section, we discuss briefly how we can treat the cases in which this assumption is not true. We

define the following general matching criterion on the two point sets, which, when minimized, solves for both the identification of landmark correspondences and their registration:

$$\mathcal{M}_{\text{geo}}(K \circ T, \Lambda) = \frac{1}{n} \sum_{i=1}^{n} \delta(T(\kappa_i), \tilde{\lambda}_i), \tag{3}$$

where $\tilde{\lambda}_i \in \Lambda$ is the "closest" point to the transformed landmark $T(\kappa_i) \in K$ and δ is a function that evaluates the distance between the two points (e.g., on the basis of Euclidean distance). In this context, the closest point $\tilde{\lambda}_i$ can indeed mean the closest one with respect to the Euclidean distance. However, it can also be with respect to another, visual similarity criterion where, for instance, the appearance of small patches centered at the landmarks is compared. We define a general way of obtaining the corresponding landmarks in Λ as

$$\tilde{\lambda}_i = \arg\min_{\lambda_j} \rho(T(\kappa_i), \lambda_j), \tag{4}$$

where ρ can be any criterion defining a distance between $T(\kappa_i)$ and λ_j.

In some applications, the correspondences are known and the cardinality of the two point sets is equal (i.e., $n = m$). In such cases, the geometric matching criterion simplifies to

$$\mathcal{M}_{\text{geo}}(K \circ T, \Lambda) = \frac{1}{n} \sum_{i=1}^{n} \delta(T(\kappa_i), \lambda_i). \tag{5}$$

The main strengths of geometric registration include its ability to cope with large deformations, the well-posed form of the minimization problem, and the guarantee of proper anatomical correspondences (if reliable landmark detection is assumed). Conversely, the detection and the correspondence tasks are far from trivial (they can be time-consuming and tedious, if manual selection is considered). Also, at the same time, the transformation inherits partial and spatially varying support during the estimation process, which might lead to an incomplete and rather sparse matching. In fact, to obtain a dense displacement field D, the displacements of image points outside the set of landmarks need to be determined through an interpolation model such as thin-plate splines. The limitations of geometric registration can be alleviated through the use of iconic registration, which assumes a one-to-one mapping between a dense set of image points.

2.2. Iconic Registration

Iconic methods perform registration by considering directly the intensities of the two images. Such methods are often considered in applications such as matching anatomical MR images to brain atlases in neuroimaging population studies (42, 43) or registering 2D images in stacks of microscope images (44). A (point-wise) matching criterion for iconic registration can be defined on the image domain Ω as

$$\mathcal{M}_{\text{ico-pw}}(I \circ T, J) = \int_{\Omega} \vartheta(I \circ T(x), J(x))\, dx, \tag{6}$$

which involves the selection of an intensity-based similarity measure ϑ. For clarity, and without loss of generality, let us explicitly define the (normalized) sum of absolute differences (SAD) measure, which is often considered in intramodal registration scenarios (for instance, for alignment of CT images). It is defined as

$$\mathcal{M}_{\text{sad}}(I \circ T, J) = \int_{\Omega} |I \circ T(x) - J(x)|\, dx. \tag{7}$$

The SAD measure is quite restrictive because it assumes that corresponding objects have the same intensities in the two images. In intermodal scenarios, such as registration of CT with MR images,

statistical similarity measures such as MI are considered. MI is commonly defined directly on the domain of the joint intensity distribution $\pi(i, j)$ as

$$\mathcal{M}_{\text{mi}}(I \circ T, J) = -\int_{\mathcal{I}} \int_{\mathcal{J}} \pi(i, j) \log \frac{\pi(i, j)}{\pi(i)\pi(j)} di\, dj, \tag{8}$$

where $\pi(i)$ and $\pi(j)$ are the marginal distributions, and $\mathcal{I}$ and $\mathcal{J}$ are the intensity domains of images $I \circ T$ and J. The corresponding point-wise definition (45) is

$$\mathcal{M}_{\text{pmi}}(I \circ T, J) = -\int_{\Omega} \log \frac{\pi(I \circ T(x), J(x))}{\pi(I \circ T(x))\pi(J(x))} dx. \tag{9}$$

The choice of the similarity measure is of great importance, and it should be made such that the chosen criterion is able to account for the intensity relation between the two images. Moreover, the properties of the function, such as its convexity, can further influence the quality of the registration. Defining an appropriate criterion is a challenging task and subject of research owing to its application and data-specific nature.

2.3. Regularization

The matching criterion can be seen as the driving force in any registration algorithm. However, adding an additional regularization term $\mathcal{R}$ is often desirable (and sometimes necessary). The regularization term allows us to impose certain constraints such as smoothness on the estimated transformation. A general regularization term for iconic registration can be defined as

$$\mathcal{R}_{\text{ico}}(T) = \alpha \int_{\Omega} \psi(T(x))\, dx, \tag{10}$$

where ψ is a function that penalizes certain properties of the dense transformation and α is a weighting parameter that controls the influence of the penalty term. An example is diffusion regularization, which is often considered in iconic registration. Diffusion regularization, in which we impose smoothness by penalizing the first-order derivatives, is defined as

$$\mathcal{R}_{\text{diff}}(T) = \alpha \int_{\Omega} ||\nabla T(x)||^2 dx. \tag{11}$$

Other regularization terms could penalize higher-order derivatives or aim at favoring deformations with local rigidity (46) or volume preservation (47). In the case of geometric registration, we can preserve the overall topology or distribution of the landmarks by regularizing the transformation on the landmarks:

$$\mathcal{R}_{\text{geo}}(T) = \frac{\alpha}{n(n-1)} \sum_{i=1}^{n} \sum_{j=1, j\neq i}^{n} ||(T(\kappa_i) - T(\kappa_j)) - (\kappa_i - \kappa_j)||. \tag{12}$$

Regularization is necessary in the case of general iconic registration because the optimization problem otherwise would be ill posed. There are d unknowns (the components of the displacement vectors) to be estimated per image point, whereas only a single observation (the intensity) is given. We discuss below that regularization also can be achieved implicitly through a parameterization of the transformation model. Still, energy-based regularization can be useful for imposing soft constraints for both iconic registration and geometric registration.

2.4. Hybrid Registration Using a Universal Coupled Formulation

Having defined the matching criteria and regularization terms for the two classes of registration, we can now define the complete energy for each class. A purely geometric (23–25) registration energy can be defined as

$$\mathcal{E}_{\text{geo}}(T) = \mathcal{M}_{\text{geo}}(K \circ T, \Lambda) + \mathcal{R}_{\text{geo}}(T), \tag{13}$$

whereas a purely iconic (13, 17, 48–51) registration energy is similarly defined as

$$\mathcal{E}_{\text{ico}}(T) = \mathcal{M}_{\text{ico}}(I \circ T, J) + \mathcal{R}_{\text{ico}}(T). \tag{14}$$

Both registration approaches have advantages and disadvantages. Iconic registration can achieve great accuracy by establishing dense correspondences. However, this approach comes with the cost of high computational effort, and by considering all image points in an equal way, it might fail to give salient points the importance they might deserve. Additionally, the solution of iconic registration often highly depends on the initial conditions such as the initial overlap domain of the two images; thus, the presence of large deformations might deteriorate the solution. This is often an issue in applications where large organ variability is expected, such as longitudinal abdominal imaging for radiation therapy (52) or population analysis for the creation of deformable, soft-tissue organ models (53).

Geometric registration can overcome some of these limitations. Given an accurate method for extracting landmarks, solving the registration problem is straightforward. Large deformations and the initial conditions have almost no influence on the final solution. However, the task of extracting reliable landmarks is not trivial, and a lot of research effort has been devoted to it. Also, geometric registration establishes direct correspondences only for a rather sparse set of points; therefore, the deformation for the remaining points needs to be interpolated. Obviously, the accuracy of the registration in the vicinity of landmarks is much higher, and it decreases for image points further away.

Hybrid registration aims to incorporate the best of both worlds. In this context, most hybrid methods separate the registration task into two successive steps. First, a geometric registration that roughly prealigns the two images is performed. Second, an iconic registration that makes use of the geometric solution and the established correspondences is performed. The result of the geometric registration can be integrated into the result of the iconic registration in one of two ways. In the first way, we can simply use the estimated transformation T_{geo} as an initialization for the iconic formulation (54):

$$\mathcal{E}_{\text{hyb}}(T) = \mathcal{M}_{\text{ico}}(I \circ T \circ T_{\text{geo}}, J) + \mathcal{R}_{\text{ico}}(T \circ T_{\text{geo}}). \tag{15}$$

In the second way, we can add the geometric matching term on the basis of preestimated landmark correspondences as in Equation (5) and encourage the result of the iconic registration to comply with that of the geometric registration (55–57):

$$\mathcal{E}_{\text{hyb}}(T) = \mathcal{M}_{\text{ico}}(I \circ T, J) + \mathcal{R}_{\text{ico}}(T) + \beta \frac{1}{n} \sum_{i=1}^{n} \delta(T(\kappa_i), \lambda_i), \tag{16}$$

where β controls the influence of the geometric term.

The problem with these two hybrid approaches is that by solving the two subproblems separately, these solutions do not really benefit from each other. Indeed, the iconic registration can profit from the prealignment or preestimation of correspondences, but the geometric registration, and the identification of correspondences in particular, could also benefit from the iconic registration. Ideally, we would like to consider the two problems in a coupled, unified way (58, 59) where the minimization of the objective function solves for both problems simultaneously.

Eventually this could result in more consistent, more accurate registration that has none of the previously mentioned limitations but accumulates all the advantages from both worlds. To this end, we define a coupled registration objective functions as

$$\mathcal{E}_{\text{uni}}(T_{\text{ico}}, T_{\text{geo}}) = \underbrace{\mathcal{M}_{\text{ico}}(I \circ T_{\text{ico}}, J) + \mathcal{R}_{\text{ico}}(T_{\text{ico}}) + \mathcal{H}(T_{\text{ico}}, T_{\text{geo}})}_{\textit{iconic}} + \underbrace{\mathcal{M}_{\text{geo}}(K \circ T_{\text{geo}}, \Lambda) + \mathcal{R}_{\text{geo}}(T_{\text{geo}})}_{\textit{geometric}}, \quad (17)$$

with $\mathcal{H}$ being a consistency term defined on T_{ico} and T_{geo}. It has the form

$$\mathcal{H}(T_{\text{ico}}, T_{\text{geo}}) = \int_{\Omega} \| T_{\text{ico}}(x) - T_{\text{geo}}(x) \| dx. \quad (18)$$

Minimizing the coupled objective function yields two transformations, which ideally are identical at the stage of convergence. Equation (17) is based on the general geometric matching term, which also involves the search for correspondences as defined in Equations (3) and (4). This coupled formulation can be seen as a universal energy formulation for the problem of deformable registration. But how can we minimize such an energy efficiently?

Existing registration methods such as gradient descent are based mainly on continuous optimization. These methods have in common that they require the differentiation of the energy function. This can be straightforward for simple energies, but it can be difficult for more complex, general energies such as the one defined in Equation (18). Additionally, continuous methods are sensitive to the initial conditions and often computationally inefficient. In fact, any change on one of the energy terms requires a careful adjustment of the optimization procedure. To overcome these limitations, we propose a discrete formulation of the registration that enables us to employ powerful combinatorial graph optimization methods. Neither analytical nor numerical differentiation is required, which makes it straightforward to plug in new energy terms or modify the existing ones. Another great advantage of discrete optimization is the inherent search in a large neighborhood, which can overcome the problem of getting stuck into local minima. Depending on the definition and size of the search range, each of which can be controlled intuitively, discrete methods are able to "jump out" of local minima. Indeed, the accuracy is bounded by the discretization, but with intelligent refinement strategies, the same accuracy of continuous methods can be achieved. First, however, the discrete formulation requires a decomposition of the continuous problem into discrete entities. This is described below.

2.5. Decomposition into Discrete Deformation Elements

An important aspect in deformable registration is the large number of parameters to be estimated. If we consider a 3D registration of moderately sized images with 256^3 voxels, the dense displacement field has more than 50 million unknowns (i.e., one 3D displacement vector per voxel). A direct optimization of the general objective function as defined in Equation (17) is inefficient. A solution to this problem is the employment of a sparse representation for the dense transformation through a compact model with a reduced number of parameters. Let us consider a set of k control points distributed along the image domain. Furthermore, let k be much smaller than the number of image points. The dense displacement field can be defined as a linear combination of control point displacements $\Phi = \{\varphi_1, \ldots, \varphi_k\}$ with $\varphi_i \in \mathbb{R}^d$ as

$$D(x) = \sum_{i=1}^{k} \omega_i(x) \varphi_i, \quad (19)$$

and the transformation T becomes

$$T(x) = x + \sum_{i=1}^{k} \omega_i(x)\varphi_i. \tag{20}$$

Here, ω_i corresponds to an interpolation or weighting function that determines the influence of a control point i to the image point x—the closer the image point, the higher the influence of the control point. The actual displacement of an image point is then computed via a weighted sum of control point displacements. A dense deformation of the image thus can be achieved by manipulating a few control points.

A popular choice for such a compact representation are FFDs (60), where the weighting functions are based on cubic B-splines and where the control points, which have only a limited local support, are uniformly distributed over the image domain in a grid-like manner. FFDs are computationally efficient and have been used successfully for medical image registration (17). In this review, we also consider FFDs as our transformation model.

By introducing such a parameterization, the registration objective changes: Instead of seeking displacement vectors for every image point, we now need to determine the displacements of the control points. Let us redefine the previous registration terms with respect to the parameterized transformation model. We start with the point-wise matching criterion for iconic registration defined in Equation (6), which, on the basis of the compact model, reads as

$$\mathcal{M}_{\text{ico-pw}}(I \circ T, J) = \frac{1}{k} \sum_{i=1}^{k} \int_{\Omega} \hat{\omega}_i(x)\vartheta(I \circ T(x), J(x))\, dx. \tag{21}$$

In Equation (21), $\hat{\omega}_i$ are weighting functions similar to the ones in Equation (20), but here the weightings determine the influence or the contribution of an image point x onto the (local) matching term of individual control points. Only image points in the vicinity of a control point are considered for the evaluation of the intensity-based similarity measure with respect to the displacement of this particular control point. This is in line with the local support that a control point has on the deformation.

For region-based and statistical measures such as cross-correlation or MI [cf. Equation (8)], the matching terms look slightly different. Here, we consider local versions of the similarity measure, and the definition for MI becomes

$$\mathcal{M}_{\text{mi}}(I \circ T, J) = -\frac{1}{k} \sum_{i=1}^{k} \int_{\mathcal{I}_{\Omega_i}} \int_{\mathcal{J}_{\Omega_i}} \pi_i(a, b) \log \frac{\pi_i(a, b)}{\pi_i(a)\pi_i(b)} da\, db, \tag{22}$$

where π_i is a local distribution for intensity domains $\mathcal{I}_{\Omega_i}$ and $\mathcal{J}_{\Omega_i}$ drawn from the patch Ω_i centered at control point i.

As in Equation (21), we now can redefine the regularization term from Equation (10) on the basis of the set of control points as

$$\mathcal{R}_{\text{ico}}(T) = \frac{\alpha}{k} \sum_{i=1}^{k} \int_{\Omega} \hat{\omega}_i(x)\psi(T(x))\, dx. \tag{23}$$

The geometric matching and regularization terms are already in discrete form because they are based on the finite set of landmarks. Still, we can rewrite the transformation consistency term from Equation (18) in a more efficient way solely on the basis of the landmarks as

$$\mathcal{H}(T_{\text{ico}}, T_{\text{geo}}) = \frac{1}{n} \sum_{i=1}^{n} \| T_{\text{ico}}(\kappa_i) - T_{\text{geo}}(\kappa_i) \|. \tag{24}$$

If we now also consider a connection between control point displacements Φ and landmark displacements, the previous relation can be rewritten as

$$\mathcal{H}(T_{\text{ico}}, T_{\text{geo}}) = \frac{1}{n}\sum_{i=1}^{n}\left\| \kappa_i + D_{\text{geo}}(\kappa_i) - \kappa_i - \sum_{j=1}^{k}\omega_j(\kappa_i)\varphi_j \right\|, \tag{25}$$

where $D_{\text{geo}}(\kappa_i) = \tilde{\lambda}_i - \kappa_i$, i.e., the displacement for the correspondence of the two landmarks κ_i and $\tilde{\lambda}_i$. If we exploit the fact that the coefficients ω_j have positive values, that their sum is $\sum_{j=1}^{k}\omega_j(x) = 1$, and that the triangular inequality holds, the coupling term can be defined as an upper bound of the previous one as

$$\mathcal{H}(T_{\text{ico}}, T_{\text{geo}}) = \frac{1}{n}\sum_{i=1}^{n}\sum_{j=1}^{k}\omega_j(\kappa_i)\| D_{\text{geo}}(\kappa_i) - \varphi_j \|. \tag{26}$$

The above redefinitions allow us to introduce our main contribution, which is the mapping of the deformable registration problem into a discrete labeling problem. This framework is based on our previous works on iconic registration (61) and geometric registration (59). The discrete entities of this problem are the set of control point displacements Φ and the two sets of landmarks K and Λ. Before demonstrating how we define the universal formulation as a graph labeling problem, let us briefly introduce the general concept behind this idea.

3. REGISTRATION VIA MARKOV RANDOM FIELD LABELING

A wide variety of tasks from the areas of computer vision, medical image analysis, and pattern recognition can be formulated as discrete labeling problems, where one seeks to optimize an objective function related to the quality of the labeling. Such problems can be elegantly expressed in the language of discrete MRFs (36), which is the reason that MRF optimization is considered to be a fundamentally important task and that it has been attracting a significant amount of research interest for more than 30 years. In this case, minimizing the energy of an MRF with unary potentials $\bar{\mathbf{g}} = \{\bar{g}_p(\cdot)\}$ and pairwise potentials $\bar{\mathbf{f}} = \{\bar{f}_{pq}(\cdot,\cdot)\}$ amounts to solving the problem

$$\text{MRF}(\bar{\mathbf{g}}, \bar{\mathbf{f}}) \equiv \min_{\mathbf{u}} \sum_{p\in V}\bar{g}_p(u_p) + \sum_{(p,q)\in E}\bar{f}_{pq}(u_p, u_q), \tag{27}$$

where each random variable u_p takes values in a discrete label set L, and V and E denote, respectively, the vertices and edges of a graph $G = (V, E)$. In practice, the unary potentials $\bar{g}_p(u_p)$ are typically used for encoding some sort of data likelihood, whereas the pairwise potentials $\bar{f}_{pq}(u_p, u_q)$ typically act as regularizers and thus play an important role in obtaining high-quality results. The latter potentials often take the form

$$\bar{f}_{pq}(u_p, u_q) = \alpha_{pq}\, d(u_p, u_q), \tag{28}$$

where α_{pq} is a per-edge weight representing the strength of relationship between adjacent vertices p and q, and $d(u_p, u_q)$ is a distance function measuring the dissimilarity between labels. The intuition behind the definition in Equation (28) is that tightly related vertices p and q should have similar labels assigned to them.

Optimization algorithms for MRFs must be able to handle energies that are as general as possible because this allows using energy functions that provide a better and more accurate modeling of the problem at hand. Of course, the difficulty of maximum a posteriori inference varies greatly for different energy types, such as different pairwise potentials. In addition to the above requirement, however, the inference algorithms must be extremely efficient because many of the problems

encountered in practice are of a large scale. We present our optimization methods in detail in Section 3.3. Let us now discuss how we can bring the universal formulation for deformable registration defined in Equation (17) into the form of an MRF objective function.

3.1. Markov Random Field Registration Energy

We have identified the discrete deformation elements of our problem as Φ (the set of control point displacements), and K and Λ (the two sets of landmarks). Now, we need to map these elements to MRF entities: the graph vertices, the edges, the set of labels, and the potential functions. Let us first introduce a graph $G_{\text{ico}} = (V_{\text{ico}}, E_{\text{ico}})$ consisting of a set of vertices V_{ico} corresponding to the set of control point displacements, i.e., $|V_{\text{ico}}| = |\Phi|$. Furthermore, a label assignment $u_p \in L_{\text{ico}}$ (with $p \in V_{\text{ico}}$) is equivalent to an update $\Delta\varphi_p$ on the control point p, i.e., $u_p \equiv \Delta\varphi_p$. So, the label set for this set of variables is $L_{\text{ico}} \subset \mathbb{R}^d$, which is a discrete version of the displacement space. We also introduce a neighborhood system E_{ico} on the vertices, which follows a common 6-connected neighborhood in 3D and a 4-connected one in 2D, corresponding to the uniform grid-like structure of the FFD transformation model. According to Equation (21), we define the unary potentials for point-wise similarity measures as

$$\bar{g}_{\text{ico},p}(u_p) = \int_{\Omega} \hat{\omega}_p(x)\vartheta(I \circ T_{\text{ico},u_p}(x), J(x))\, dx, \tag{29}$$

where T_{ico,u_p} denotes the transformation where control point p has been updated by u_p. Region-based and statistical measures are again encoded in a similar way on the basis of local evaluation of the similarity measure. The MI, for example, is encoded as

$$\bar{g}_{\text{ico},p}(u_p) = -\int_{\mathcal{I}_{\Omega_p}} \int_{\mathcal{J}_{\Omega_p}} \pi_p(a,b) \log \frac{\pi_p(a,b)}{\pi_p(a)\pi_p(b)} da\, db. \tag{30}$$

The definition of the matching criterion on the unary potentials can be only an approximation to the real matching energy. The problem here is that on unary potentials, we assume conditional independence between the random variables. However, the image deformation and thus the local similarity measure depend on more than one control point because their influence areas overlap. Still, the above approximation yields accurate registration, as we show below. Furthermore, it allows an extremely efficient approximation scheme, which is described in the next section.

The compact regularization term defined in Equation (23) could be defined as well in the above manner. However, this not very efficient because the penalties need to be computed on the dense field for every variable and every label. If we consider the diffusion regularization as defined in Equation (11), we can employ an efficient discrete approximation of this term on the basis of pairwise potentials as

$$\bar{f}_{\text{diff},pq}(u_p, u_q) = \alpha_{pq} \frac{||(\varphi_p + u_p) - (\varphi_q + u_q)||}{||p - q||}. \tag{31}$$

The pairwise potentials penalize deviations of displacements of neighboring control points $(p, q) \in E_{\text{ico}}$, which is an approximation to penalizing the first derivatives of the transformation. We also can remove the current displacements φ_p and φ_q from the above definition, yielding a term that penalizes only the updates on the deformation. This would change the behavior of the energy from an elastic-like to a fluid-like regularization. This choice depends on the application, but for medical imaging, we commonly prefer the elastic-like behavior.

Let us now introduce a second graph $G_{\text{geo}} = (V_{\text{geo}}, E_{\text{geo}})$ for the geometric entities K and Λ. The most general case of geometric registration is considered—that is, the one where the two sets of landmarks have different cardinalities. We seek the transformation that will bring each

landmark into correspondence with the best candidate (the closest with respect to a matching criterion). Equivalently, we can state that we are trying to solve for the correspondence of each landmark, which naturally results in a set of sparse displacements.

The second graph consists of a set of vertices V_{geo} corresponding to the set of landmarks extracted in the source image, i.e., $|V_{\text{geo}}| = |K|$. A label assignment $u_p \in L_{\text{geo}} := \Lambda$ (where $p \in V_{\text{geo}}$) is equivalent to matching the landmark $\kappa_p \in K$ to a candidate point $u_p \equiv \lambda$. Assigning a label u_p implicitly defines a displacement $D_{\text{geo},u_p}(\kappa_p) = u_p - \kappa_p$ because κ_p is mapped on the landmark u_p. According to Equations (3) and (4), the unary potentials are defined as

$$\bar{g}_{\text{geo},p}(u_p) = \int_{\Omega_{u_p}} \rho(I \circ T_{\text{geo},u_p}(x), J(x))\, dx, \tag{32}$$

where Ω_{u_p} denotes a patch around the point u_p. The unary potentials determine the likelihood of two points being matched by evaluating the dissimilarity over patches centered around them.

The regularization term defined in Equation (12) can be encoded by the edge system E_{geo} of the graph. In this setting, the regularization term can be expressed as

$$\bar{f}_{\text{geo},pq}(u_p, u_q) = \alpha_{pq} ||(T_{\text{geo},u_p}(\kappa_p) - T_{\text{geo},u_q}(\kappa_q)) - (\kappa_p - \kappa_q)||. \tag{33}$$

The pairwise potential will enforce an isometric property. Having performed an affine registration step to account for scale differences as preprocessing, we suppose that the geometric distance between homologous points in the two images does not vary too much. Moreover, if the vector differences are considered, flipping of the point positions is penalized.

The last missing term of the universal registration energy is the coupling penalty [cf. Equation (26)]. We introduce a third set of edges E_{hyb} containing all possible connections between the iconic random variables and the geometric variables. The pairwise label assignment penalty on these coupling edges is then defined as

$$\bar{f}_{\text{hyb},pq}(u_p, u_q) = \omega_q(\kappa_p) \| D_{\text{geo},u_p}(\kappa_p) - (\varphi_q + u_q) \|, \tag{34}$$

where $p \in V_{\text{geo}}$ and $q \in V_{\text{ico}}$, $u_p \in L_{\text{geo}}$ and $u_q \in L_{\text{ico}}$, and $(p, q) \in E_{\text{hyb}}$. Such a pairwise term couples the displacements given by the two registration processes and imposes consistency. The coupled registration objective function [cf. Equation (17)] is finally represented by an MRF graph $G_{\text{hyb}} = (V_{\text{geo}} \cup V_{\text{ico}}, E_{\text{geo}} \cup E_{\text{ico}} \cup E_{\text{hyb}})$ with its associated unary and pairwise potential functions.

Whereas the geometric registration is inherently more of a discrete nature, the iconic registration is originally a highly continuous problem. A naive discrete implementation of this problem might get easily intractable or inefficient. First, how to define a reasonable set of discrete labels that represents an n-dimensional continuous search space is not obvious. Second, the evaluation of the potential functions needs to be efficient to benefit from the computational power of discrete optimization methods. Both aspects are addressed in the following.

3.2. Efficient Approximation Scheme for Iconic Potentials

Let us have another look at the unary potentials for the iconic registration. To compute Equation (29), we need to determine the transformation under the constraint that control point p has been updated by the displacement $u_p \equiv \Delta\varphi_p$. If we do this for every control point and every discrete label, the evaluation of the MRF matching term becomes computationally expensive. However, we already discussed the fact that the unary energies will always be approximations to the real energies owing to the conditional dependence of control points with respect to the deformation. To take advantage of this, we propose the following efficient approximation scheme. Consider a label $l \in L_{\text{ico}}$ corresponding to an update $\Delta\varphi$. We first apply this displacement globally to

the source image in terms of a global translation and then compute the unary potentials for this particular label and all control points simultaneously. Thus, we need to iterate only once through the image and distribute the local energies for the control points. The constrained transformation in the unary potentials is then simply defined as $T_{\text{ico},u_p}(x) = T_{\text{ico}}(x) + u_p$, where $T_{\text{ico}}(x)$ is the current or initial estimate of the transformation. In fact, this approximation scheme can be seen as a local block matching strategy encoded on the unaries, whereas explicit smoothness is gained from the pairwise potentials and implicit smoothness is gained from the interpolation strategy.

3.3. Discrete Optimization

What remains to be described is the optimization algorithm that is used to minimize the aforementioned energy. Let us first give a brief overview of the existing methods before describing the ones that we use.

Initially, methods based on either greedy strategies (62–64) or iterative ones (65) were used. These methods suffered from either slow convergence or the lack of optimality guarantees. Graph-cut-based techniques (66), belief propagation methods (67), and LP methods (68) were proposed to remedy the aforementioned shortcomings, and they revitalized interest in the field.

Discrete optimization techniques can be separated into two classes: graph-cut-based methods and message-passing methods. Graph-cut-based methods are based on the max-flow min-cut principle (69). Computational performance (70, 71, 72, 73) is the main strength of these methods, whereas constraints (74) on the type of energies that can be minimized is their main bottleneck. The second class of methods is based on local message exchanges between the nodes of the graph to recover the best solution (75–78). The main strengths of this second class of methods are their ability to deal with arbitrary structure graphs and nonsubmodular pairwise interactions while converging to satisfactory solutions.

Continuing, we present the two methods that we used to infer the parameters of the presented discrete models. The first one is applied in the case of iconic registration as it is able to answer best the trade-off for efficiency and quality with respect to the obtained solution. The second method is able to provide better-quality solutions at the expense of higher computational time and is used in the case of the coupled model where the graph structure is more complex and the problem more difficult.

3.3.1. Fast primal-dual strategies for Markov random field optimization. Fast primal-dual (FastPD) is a recently proposed MRF optimization algorithm whose theoretical setting rests on the duality theory of LP and, in particular, on a method known as the primal-dual schema. This schema is applied as follows: MRF optimization is first cast as a linear integer program, and then one makes use of the complementary slackness conditions associated with the corresponding pair of primal and dual LP relaxations to derive solutions that attain a small primal-dual gap. For a detailed description of FastPD, we refer the interested reader to References 68 and 79. In the following, we simply mention a few of its nice properties that make it a perfect candidate for our image registration task.

1. Generality: FastPD can handle a wide class of MRFs because it merely requires $\bar{f}_{pq}(\cdot,\cdot) \geq 0$. Hence, when this algorithm is used, our image registration framework can automatically incorporate any similarity metric as well as a wide class of smoothness penalty functions.
2. Optimality: Furthermore, FastPD can always guarantee that the generated solution will be an f-approximation to the true optimum, where $f = 2\frac{d_{\max}}{d_{\min}}$.
3. Per-instance approximation factors: In fact, in addition to the aforementioned worst-case approximation factor, FastPD also can continuously update a per-instance approximation

factor during its execution. In practice, this factor drops to 1 quickly, thus allowing the global optimum to be found up to a user/application bound.

4. Speed: Finally, FastPD provides great computational efficiency because it can reach an almost optimal solution quickly and efficiently.

3.3.2. Cycle repairing and tighter linear programming relaxations. Although FastPD is considered one of the most computationally efficient optimization methods, its performance is compromised when the underlying LP relaxation used by this algorithm is not tight—that is, when it does not approximate well the original optimization problem MRF $(\bar{\mathbf{g}}, \bar{\mathbf{f}})$. To address this issue, one can rely on more efficient properties methods based on message passing, such as the sequential tree-reweighted (77) method or dual decomposition (78). Another alternative is to consider tighter relaxations like the ones used in the framework described in Komodakis & Paragios (80). An important characteristic of this framework is that the strengthening of the LP relaxations used for approximating the problem MRF $(\bar{\mathbf{g}}, \bar{\mathbf{f}})$ takes place not in the primal domain, which would be inefficient, but in the dual domain. The result of this strengthening procedure is that a hierarchy of ever tighter dual relaxations is constructed; this hierarchy starts from the same dual relaxation used by FastPD and goes all the way up to a dual relaxation that coincides with the original problem MRF $(\bar{\mathbf{g}}, \bar{\mathbf{f}})$. From this hierarchy, the authors (80) show how to handle efficiently one particular class of relaxations known as cycle relaxations. This can be achieved via a fast dual-based operation referred to as cycle repairing, which aims to deal with a difficulty that lies at the heart of MRF optimization: the existence of so-called inconsistent cycles. As the name of that operation reveals, its role is to eliminate any such cycles that may appear during optimization. Furthermore, the underlying relaxation becomes tighter as the number of cycles getting repaired grows larger. For a detailed description of the cycle-repairing framework, we refer the interested reader to Reference 80.

3.4. Iterative Labeling and Search-Space Refinement

Two important aspects in the discrete formulation need further consideration. First, the search space is finite, and the registration accuracy via labeling thus is bounded by the range of deformations covered in the set of labels. Second, the aforementioned approximations in the energy terms might yield suboptimal correspondences. Our solution to both issues is to perform iterative labeling combined with a search-space refinement strategy. Each iteration consists of computing the maximum a posteriori labeling of the MRF with respect to a certain label space; this computation yields an update on the transformation. This update is applied to the current estimate, and the subsequent iteration continues the registration on the basis of the updated transformation. Thus, the error induced by the approximation stays small, and incorrect matches can be corrected in the next iteration. Furthermore, the overall domain of possible deformations is bounded by the number of iterations rather than the set of finite labels.

The iterative labeling allows us to keep the label set quite small, which is important for efficient optimization. Additionally, we introduce a refinement on the search space in which we start with a set of larger deformations. We commonly employ a sparse sampling with a fixed number of samples s. We uniformly sample displacements along certain directions up to a maximum displacement magnitude $\delta_{\max}$. The total number of labels in each iteration is then $|L_{\text{ico}}| = g \cdot s + 1$, including the zero displacement, and g is the number of sampling directions. If the energy decreases sufficiently, we keep the current set of labels for the next iteration. If the energy does not decrease, the label space is rescaled by a factor f, where $0 < f < 1$. The next iteration is then performed on this refined search space.

The number of sampling directions g and their orientations depend on the dimensionality of the registration. One possibility is to sample just along the main coordinate axes—i.e., in positive and negative directions of the x, y, and z axes (in the case of 3D). Additionally, we can add samples along diagonal axes, for instance. In 2D, we commonly prefer a star-shape sampling, which turns out to be a good compromise between the number of samples and the sampling density. In our experiments, we also found that sparse samplings, such as samplings just along the main axes, give accurate registration results but might increase the total number of iterations needed until convergence. However, a single iteration is much faster to compute when the label set is small. In all our experiments, we find that small label sets provide excellent performance in terms of computational speed and registration accuracy.

4. EXPERIMENTAL VALIDATION

In this section, we discuss some practical considerations and details of the implementation of our registration approach. Then we present some recent results on a medical registration scenario of 4D CT data for purely iconic registration. Regarding the coupled geometric registration, results on a multimodal synthetic data set are presented. Further experimental results for a variety of other medical registration settings can be found in our earlier works on multimodal registration (81), atlas-based segmentation via registration (82), deformable stitching for whole-body MRI (83), and other topics (31, 59, 61, 84, 85). Our discrete framework for registration is of particular interest in applications with critical time constraints. We could, for instance, show that the same accurate registration was achieved in a few minutes where previous methods took hours of computation (61). This enables the use of nonrigid registration in intraoperative settings, for instance, where the motion between pre- and intraoperative images needs to be estimated rapidly. Additionally, we see a great benefit in the modularity of our approach. All kinds of complex matching criteria can be encoded easily because their differentiability does not need consideration. This is of interest in multimodal scenarios where the matching relies on highly nonlinear or statistical measures.

4.1. Implementation Details

Our implementation considers FFDs with cubic B-spline basis functions and control points uniformly distributed over the image domain as the compact transformation model. We employ a common hierarchical coarse-to-fine strategy where the resolution of both the images and the FFD control grid is subsequently refined during the registration process. For the images, we use Gaussian image pyramids with a scale factor of 2 and standard deviation of 1. The initial control point spacing is set in millimeters according to the expected maximum amount of deformation. With increasing image resolution, we halve the FFD spacing by inserting new control points, which allows us to recover larger deformations in the beginning and smaller, more subtle ones in later iterations.

Regarding the discrete label space L_{ico} for the iconic part, in all our experiments, we use a sparse sampling of the deformation space where samples are taken only along the positive and negative main axes of the 3D coordinate system. We set the number of samples $s = 5$, yielding 31 labels in total (including the zero displacement). The initial maximum displacement magnitude on each grid resolution level is coupled to the control point spacing h by setting $\delta_{\max} = 0.4 \cdot h$. This is motivated by the fact that composing the single updates on the transformation bounded to this maximum displacement yields diffeomorphic transformations (86). After each iteration, which corresponds to one MRF labeling computation, we rescale the set of labels with a fixed factor of $f = 0.66$. On each level, we commonly perform five iterations before increasing the image

and grid resolution. This strategy allows for small label sets that can be optimized efficiently, whereas the successive refinement allows submillimeter registration accuracy as demonstrated in the following experiments.

4.2. Iconic Registration

Validating the performance of the proposed framework is accomplished through the use of a 4D CT image data set of the thorax (87). It consists of a time series of 10 consecutive volumes, each of which has a size of $482 \times 360 \times 141$ voxels and a physical resolution of approximately $0.977 \times 0.977 \times 2$ mm. Each volume captures a different stage of the breathing cycle. The images are made publicly available by the Lon Brard Cancer Center and Creatis lab in Lyon, France. For more information, we refer to the Web site of the data set (**http://www.creatis.insa-lyon.fr/rio/popi-model/**).

The choice of this data set is motivated by the fact that point correspondences between images are provided, allowing for a gold-standard quantitative evaluation of the registration accuracy. Moreover, the performance of two other standard methods is provided: One is an implementation of the Demons algorithm (88), and the other one is an FFD-based approach using continuous optimization (89). Comparing with these other methods on the same data set enables us to draw conclusions with respect to the performance of our approach. To provide a fair comparison, we perform our registration on the same downsampled and cropped images as the two other methods. The physical resolution is $2 \times 2 \times 2$ mm, yielding volumes with $235 \times 176 \times 141$ voxels each.

All registrations are with respect to a fixed reference image that corresponds to the end-inhalation phase of the breathing cycle. Forty anatomical landmarks are provided, and these have been identified by medical experts in all images. After registration, we warp the landmarks using the resulting deformation field and compute the target registration error (TRE) between the warped and manual landmarks. The TRE is simply the Euclidean distance (in millimeters) between corresponding landmarks.

Our first set of experiments involves purely iconic registration. Owing to the monomodality of the data, we use the SAD matching criterion. Additionally, we use the diffusion regularization with elastic-like behavior. The weighting between these two terms is uniformly set to $\alpha_{pq} = 5$. We further employ a hierarchical setting with four resolution levels, for both the images and the FFD control grid. The initial control point spacing is set to 40 mm and subsequently refined to 20, 10, and 5 mm. Each of the nine registrations takes less than 7 min on an Intel® Xeon® Quad-Core 2.27 GHz CPU. Much higher run times (>30 min) are reported for the two other methods (the Demons algorithm and the FFD-based approach), but because of the different systems used for the registration, these numbers are not directly comparable. If we look at the registration accuracy in terms of TRE (see **Table 1**), we see that our iconic MRF approach performs best with an average TRE for all registrations of less than 1 mm. This is quite remarkable given the downsampled resolution of 2-mm voxel size. We also see that for the images that are very close to the reference scan (images 1 and 2 have an initial TRE of less than 0.5 mm), the two other methods deteriorate the alignment, whereas our method preserves the initial accuracy quite well. Visual results for one specific case (image 4) are shown in **Figures 1** and **2**.

4.3. Coupled Registration

To validate the coupled geometric registration method, a multimodal synthetic data set is used. In this setting, the ground-truth deformation is known, allowing for a quantitative analysis of the registration performance regarding both the dense deformation field accuracy and the quality of the established landmark correspondences.

Table 1 Target registration errors (in millimeters) for the registration of the 4D CT data set

	Initial			Demons algorithm			Free-form deformation			Ours (iconic)		
Image	Mean	Std	Maximum	Mean	Std	Maximum	Mean	Std	Maximum	Mean	Std	Maximum
1	0.48	0.54	2.36	1.29	0.31	1.82	0.80	0.29	1.37	**0.56**	0.32	1.78
2	0.49	0.62	2.57	1.36	0.26	2.20	0.81	0.47	2.01	**0.59**	0.45	1.90
3	2.19	1.84	6.56	1.36	0.46	2.52	1.13	0.51	2.34	**1.05**	0.55	2.48
4	4.33	2.54	10.01	1.23	0.48	3.02	1.12	0.43	2.02	**1.09**	0.53	2.64
5	5.75	2.67	12.03	1.30	0.49	2.62	**1.15**	0.60	2.81	1.17	0.62	3.05
6	6.10	2.96	14.01	**1.14**[a]	0.43	2.13	1.24	0.60	3.03	1.19	0.50	2.34
7	5.03	2.36	12.23	1.28	0.52	2.48	1.21	0.72	2.96	**1.16**	0.69	2.89
8	3.68	1.59	6.21	1.11	0.30	1.66	**0.91**	0.47	2.14	0.92	0.46	2.18
9	2.07	1.07	4.49	1.09	0.32	1.75	0.95	0.44	2.16	**0.86**	0.50	2.14
All	3.35	2.82	14.01	1.24	0.42	3.02	1.04	0.53	3.03	**0.96**	0.57	3.05

[a] Boldface font indicates best performance.
Abbreviation: Std, standard deviation.

Starting from a coregistered pair of T1-T2 brain images of size $256 \times 256 \times 48$ voxels and of physical resolution equal to $0.9375 \times 0.9375 \times 3$ mm, 10 target images were generated from the 3D T2 MRI image. The deformation fields are created by composing two different configurations of FFD grids. The first one has a control spacing equal to $h = 48$ mm, resulting in coarse deformations, whereas the second one, with a control spacing of $h = 18$ mm, is responsible for more local deformations. The different configurations of the FFD grids are produced by random movement of the grid nodes in all three dimensions. The maximum displacement that the grid nodes can perform is bounded such that the resulting deformation is diffeomorphic. That is, for the first grid, it is equal to 19.2 mm; for the second one, it is 7.2 mm. In each of the 10 generated images, 300–400 landmarks positioned in salient image regions were selected manually. The landmark set K consists of these points. Given the deformation fields, for each point of interest in the target image domain, its homolog in the source image domain can be determined. Around each homologous point, nine points are selected randomly. These points, along with the true correspondence, form the set of the candidate landmarks Λ.

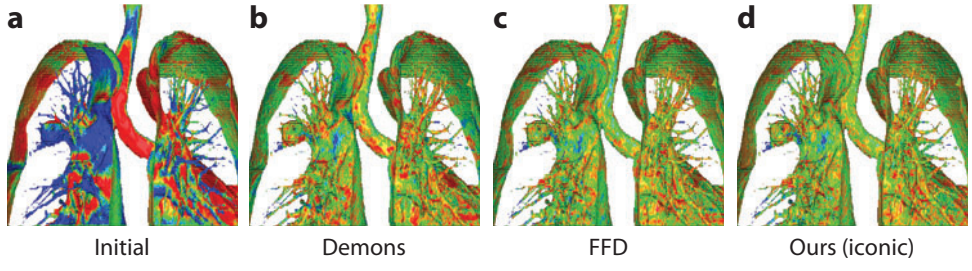

Figure 1

Color-encoded surface distance in the lung area (*a*) before and (*b–d*) after registration of image 4 (see **Table 1**). (*a*) Initial conditions. (*b*) After use of the Demons algorithm. (*c*) After use of the free-form deformation (FFD) approach using continuous optimization. (*d*) After use of our iconic method. Dark blue and dark red correspond to distances >1.5 mm, and green corresponds to distances close to zero.

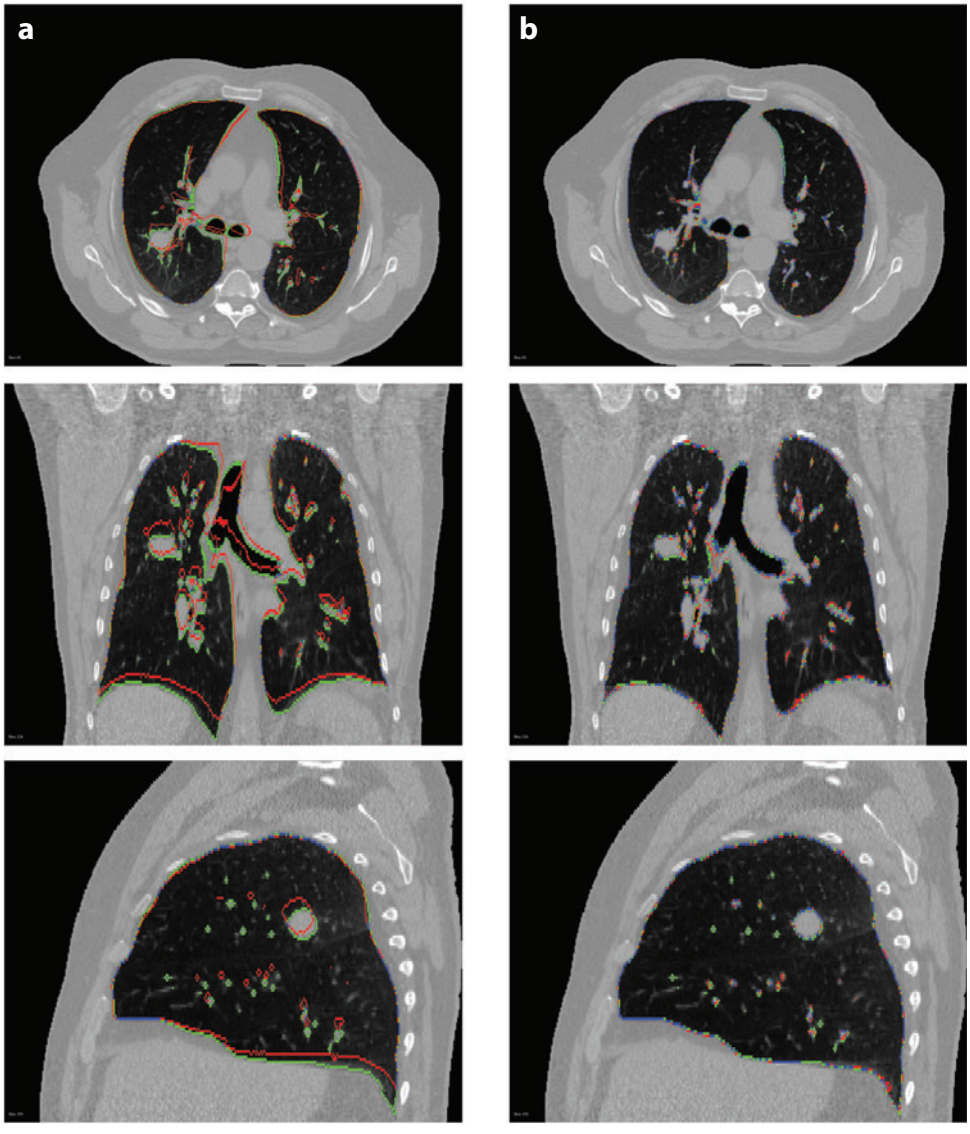

Figure 2

Visual results (*a*) before and (*b*) after registration of image 4 using our iconic approach. Green voxels correspond to the segmentation of the reference; red voxels, to the (warped) segmentation of image 4. Voxels in blue show exact overlap of reference and warped segmentation.

In this experimental setting, the initial T1 image is used as the source and is registered to the generated T2 ones. Once the registration task is performed, the estimated deformation field is compared with the one that was used to create the images. The difference between the two deformation fields is quantified by measuring the end-point error and the angular error. Voxels that belong to the background are ignored during these calculations. The end-point error is measured in millimeters and is simply the Euclidean distance between the two 3D motion vectors. The angular error between the two motion vectors is the angle between them. It can be computed

Table 2 End-point errors (in millimeters) for the registration of the synthetic magnetic resonance data set

	Iconic (h = 60 mm)		Hybrid (h = 60 mm)		Iconic (h = 20 mm)		Hybrid (h = 20 mm)	
Image	Mean	Std	Mean	Std	Mean	Std	Mean	Std
1	1.33	0.69	**1.25**[a]	0.59	1.38	1.21	**0.98**	0.61
2	1.32	0.75	**1.18**	0.53	2.46	3.21	**1.06**	0.68
3	1.44	0.97	**1.22**	0.56	2.05	2.40	**1.03**	0.67
4	1.40	0.74	**1.16**	0.50	1.40	1.02	**1.08**	0.69
5	1.23	0.60	**1.15**	0.56	1.38	1.01	**1.03**	0.67
6	1.35	0.74	**1.24**	0.62	1.58	1.39	**1.05**	0.71
7	1.16	0.56	**1.09**	0.50	1.45	1.18	**1.05**	0.67
8	1.29	0.68	**1.23**	0.58	1.93	2.61	**1.11**	0.79
9	1.23	0.62	**1.19**	0.53	1.72	1.89	**1.04**	0.71
10	1.54	1.08	**1.19**	0.58	2.60	3.43	**1.05**	0.73
All	1.33	0.11	**1.19**	0.05	1.79	0.45	**1.05**	0.03

[a]Boldface font indicates best performance.
Abbreviation: Std, standard deviation.

by calculating the inner product between the normalized vectors and then calculating the inverse cosine. The use of these error measurements is common in the literature of optical flow (90).

Given the multimodal nature of the data, the MI is used as the iconic criterion. Regarding the regularization term of the iconic graph, the diffusion regularization with fluid-like behavior is preferred because it leads to faster computations. The pairwise terms modeling the diffusion regularization are weighted by a factor of 0.01. As our main interest is to outline the potential of the proposed coupled approach, the matching criterion for the case of the geometric registration is based on the Euclidean distance between the true correspondence and the point indexed by the label at hand. The unary potentials are multiplied by 10. Regarding the pairwise potential for the geometric case, the one presented in Equation (33) is used as is. Last, but not least, the weight for the coupling term in Equation (34) is set to 0.01. A hierarchical setting similar to the one used for the experimental validation of the iconic method is used, with the difference that three resolution levels are employed with an initial control point spacing equal to 60 mm. Each registration takes ~15 min on an Intel® Xeon® X5680 3.33 GHz CPU.

If we look at the registration accuracy in terms of end-point and angular errors (see **Tables 2** and **3**), we see that our coupled iconic-geometric registration method is able to further ameliorate the results of the iconic one. This is evident from the fact that both the end-point and angular errors decreased when the geometric information was utilized. Because we expect the hybrid approach to be able to cope with large displacements better than the pure iconic one does, we repeated the experiments by decreasing the initial control point spacing to 20 mm and thus limiting the maximum amount of deformation that can be handled. The results are also reported in **Tables 2** and **3**. In this case, we can observe a more significant difference between the performances of the two proposed approaches. Therefore, we should conclude that the additional computational cost demanded by the coupled approach can be compensated by the better quality of the results. Visual results for one specific case are displayed in **Figure 3**, which shows a checkerboard image that is created by interchanging parts of the two images. It is evident from the difference between the neighboring tiles that the images differ greatly before the registration. The continuity of the patterns across neighboring tiles suggests that the images have been aligned. No significant visual

Table 3 Angular errors (in degrees) for the registration of the synthetic magnetic resonance data set

	Iconic (b = 60 mm)		Hybrid (b = 60 mm)		Iconic (b = 20 mm)		Hybrid (b = 20 mm)	
Image	Mean	Std	Mean	Std	Mean	Std	Mean	Std
1	8.70	6.66	**8.18**[a]	6.16	8.25	8.92	**6.08**	5.12
2	6.85	4.37	**6.43**	4.32	13.89	23.73	**5.13**	3.93
3	10.40	10.52	**8.50**	7.76	14.02	17.12	**7.34**	7.29
4	14.46	11.50	**11.69**	10.24	14.61	14.34	**11.49**	11.72
5	7.65	7.79	**7.23**	7.93	8.31	9.32	**6.17**	6.97
6	8.20	7.08	**7.21**	6.16	9.85	13.64	**6.13**	6.13
7	10.19	11.20	**9.50**	10.19	12.01	15.06	**8.67**	9.69
8	8.67	9.75	**8.01**	8.49	10.87	15.14	**6.69**	7.58
9	9.60	9.19	**8.84**	8.014	13.62	19.06	**8.03**	8.95
10	13.12	14.43	**11.03**	12.64	17.42	20.26	**9.24**	11.15
All	9.78	2.39	**8.66**	1.68	12.29	2.97	**7.50**	1.90

[a]Boldface font indicates best performance.
Abbreviation: Std, standard deviation.

difference can be observed between the result obtained with the pure iconic method and that obtained with the coupled approach.

5. DISCUSSION

This review presents a novel theoretical framework for deformable image registration based on a discrete formulation in terms of graph labeling and recent advances in discrete optimization. The method relies on an efficient pairwise MRF formulation and is generic and modular with respect to the registration objective function. Our contributions are threefold: (*a*) Our method is able to handle a wide range of matching criteria, and energy terms are easily interchangeable because no differentiation is needed; (*b*) the general formulation allows us to consider different types of transformation models as long as a mapping to discrete entities is possible (which is the case for

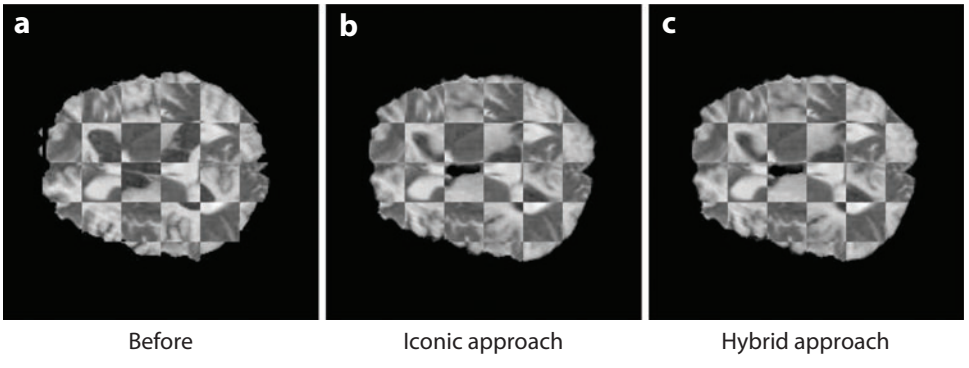

Figure 3

Visual results (*a*) before and (*b*,*c*) after registration of image 2 using the proposed (*b*) iconic and (*c*) hybrid approach. The results are given in the form of a checkerboard, where neighboring tiles come from different images.

most parametric models); and (*c*) we integrate both geometric and iconic support in a principled and unified formulation through joint optimization of interconnected random variables. Furthermore, we adopt two novel optimization techniques: One provides the best compromise between computational complexity and quality of the obtained solution, and the other is able to solve complex and difficult MRF problems through tight relaxations. Promising results demonstrate the potential of our method. The presented framework is of particular interest in applications where computation time is a critical issue (for instance, in intraoperative imaging) or where the variation in data is huge and thus demands complex and application-specific matching criteria (for instance, in large-scale multimodal population studies).

The use of discrete MRFs and pairwise interactions allows feasible local decomposition of the problem and consequently parallel implementations of the registration method in terms of both energy evaluation and optimization. To this end, the use of graphic processing units and message-passing algorithms could produce near-real-time registration, a direction that is currently under investigation. Image metric regression is another potential direction (33) where we seek to replace conventional image similarity measures with application-specific ones that are learned from the clinical data. The modeling of missing correspondences is also an interesting direction, in particular when seeking registration between diseased cases and normal reference volumes for statistical modeling or when studying longitudinal evolution of diseases (such as tumor growth). Proper selection of geometric landmarks could improve registration performance and make the method insensitive to the initial conditions. This is also under investigation. The ability to provide quantitative measurements (such as uncertainties) for the energy minimization process can facilitate a clinical interpretation. For instance, regions with high registration uncertainty could be highlighted because they might correspond to large variations in the images. Such information also might be used for improving the performance of discrete optimization methods (91). Incorporating prior knowledge into the MRF topology could further improve the registration accuracy in certain scenarios (92). Last, but not least, the use of higher-order interactions within MRF formulations could either improve performance through more appropriate regularization constraints (93) or eliminate the need for linear (rigid or affine) registration prior to deformable registration.

DISCLOSURE STATEMENT

The authors are not aware of any affiliations, memberships, funding, or financial holdings that might be perceived as affecting the objectivity of this review.

ACKNOWLEDGMENTS

We would like to acknowledge the contributions of Nassir Navab (Technische Universität München, Germany), George Tziritas (University of Crete, Greece), and Yangming Ou and Christos Davatzikos (University of Pennsylvania, USA). This work has been partially supported from the sterEOS+ grant of the Medicen Ile-de-France Competitive Cluster. N.P. was partially supported by the European Community's Seventh Framework Programme, ERC grant 259112 (DIOCLES).

LITERATURE CITED

1. Osman N, Kerwin W, McVeigh E, Prince J. 1999. Cardiac motion tracking using CINE harmonic phase (HARP) magnetic resonance imaging. *Magn. Reson. Med.* 42(6):1048–60

2. Fütterer J, Heijmink S, Scheemen T, Veltman J, Huisman H, et al. 2006. Prostate cancer localization with dynamic contrast-enhanced MR imaging and proton MR spectroscopic imaging. *Radiology* 241:449–58
3. Pelizzari CA, Chen GT, Spelbring DR, Weichselbaum RR, Chen CT. 1989. Accurate three-dimensional registration of CT, PET, and/or MR images of the brain. *J. Comput. Assist. Tomogr.* 35(1):20–26
4. Kyriacou SK, Davatzikos C, Zinreich SJ, Bryan RN. 1999. Nonlinear elastic registration of brain images with tumor pathology using a biomechanical model. *IEEE Trans. Med. Imaging* 18(7):580–92
5. Mohamed A, Zacharaki EI, Shen D, Davatzikos C. 2006. Deformable registration of brain tumor images via a statistical model of tumor-induced deformation. *Med. Image Anal.* 10(5):752–63
6. Collins DL, Neelin P, Peters TM, Evans AC. 1994. Automatic 3D intersubject registration of MR volumetric data in standardized Talairach space. *J. Comput. Assist. Tomogr.* 18(2):192–205
7. Fox NC, Freeborough PA. 1997. Brain atrophy progression measured from registered serial MRI: validation and application to Alzheimer's disease. *J. Magn. Reson. Imaging* 7:1069–75
8. Crum WR, Scahill RI, Fox NC. 2001. Automated hippocampal segmentation by regional fluid registration of serial MRI: validation and application in Alzheimer's disease. *NeuroImage* 13(5):847–55
9. Risser L, Vialard F, Wolz R, Holm D, Rueckert D. 2010. Simultaneous fine and coarse diffeomorphic registration: application to the atrophy measurement in Alzheimer's disease. *Proc. Med. Image Comput. Comput. Assist. Interv., 13th, Part II, Beijing*, pp. 610–17. Berlin/Heidelberg: Springer-Verlag
10. Kessler ML. 2006. Image registration and data fusion in radiation therapy. *Br. J. Radiol.* 79:S99–108
11. Nimsky C, Ganslandt O, Hastreiter P, Fahlbusch R. 2001. Intraoperative compensation for brain shift. *Surg. Neurol.* 56(6):357–64
12. Hajnal JV, Hill DLG, Hawkes DJ, eds. 2001. *Medical Image Registration*. Boca Raton, FL: CRC
13. Modersitzki J. 2004. *Numerical Methods for Image Registration*. Oxford, UK: Oxford Univ. Press
14. Maintz JBA, Viergever MA. 1998. A survey of medical image registration. *Med. Image Anal.* 2(1):1–36
15. Zitova B, Flusser J. 2003. Image registration methods: a survey. *Image Vis. Comput.* 21(11):977–1000
16. Szeliski R. 2006. Image alignment and stitching: a tutorial. *Found. Trends Comput. Graph. Vis.* 2(1):1–104
17. Rueckert D, Sonoda LI, Hayes C, Hill DLG, Leach MO, Hawkes DJ. 1999. Nonrigid registration using free-form deformations: application to breast MR images. *IEEE Trans. Med. Imaging* 18:712–21
18. Rohr K, Stiehl H, Sprengel R, Buzug T, Weese J, Kuhn M. 2001. Landmark-based elastic registration using approximating thin-plate splines. *IEEE Trans. Med. Imaging* 20:526–34
19. Fornefett M, Rohr K, Stiehl HS. 1999. Elastic registration of medical images using radial basis functions with compact support. *Proc. Comput. Vis. Pattern Recognit., June 23–25, Fort Collins, Colo.*, pp. 402–7. Piscataway, NJ: IEEE
20. Xuan J, Wang Y, Freedman MT, Adali T, Shields P. 2006. Nonrigid medical image registration by finite-element deformable sheet-curve models. *Int. J. Biomed. Imaging* 2006:1–9
21. Arsigny V, Pennec X, Ayache N. 2003. Polyrigid and polyaffine transformations: a new class of diffeomorphisms for locally rigid or affine registration. *Proc. Med. Image Comput. Comput. Assist. Interv., 6th, Part II, Montreal*, pp. 829–37. Berlin/Heidelberg: Springer-Verlag
22. Lowe DG. 2004. Distinctive image features from scale-invariant keypoints. *Int. J. Comput. Vis.* 60(2):91–110
23. Joshi SC, Miller MI. 2000. Landmark matching via large deformation diffeomorphisms. *IEEE Trans. Image Process.* 9(8):1357–70
24. Shen D, Davatzikos C. 2002. HAMMER: hierarchical attribute matching mechanism for elastic registration. *IEEE Trans. Med. Imaging* 21(11):1421–39
25. Chui H, Rangarajan A. 2003. A new point matching algorithm for non-rigid registration. *Comput. Vis. Image Underst.* 89(2–3):114–41
26. Bookstein FL. 1989. Principal warps: thin-plate splines and the decomposition of deformations. *IEEE Trans. Pattern Anal. Mach. Intell.* 11:567–85
27. Roche A, Malandain G, Pennec X, Ayache N. 1998. The correlation ratio as a new similarity measure for multimodal image registration. *Proc. Med. Image Comput. Comput. Assist. Interv., 1st, Cambridge, Mass.*, pp. 1115–24. Berlin/Heidelberg: Springer-Verlag
28. Maes F, Collignon A, Vandermeulen D, Marchal G, Suetens P. 1997. Multimodality image registration by maximization of mutual information. *IEEE Trans. Med. Imaging* 16:187–98

29. Viola P, Wells W. 1997. Alignment by maximization of mutual information. *Int. J. Comput. Vis.* 24:137–54
30. Chung ACS, Wells WM III, Norbash A, Grimson WEL. 2002. Multi-modal image registration by minimizing Kullback-Leibler distance. *Proc. Med. Image Comput. Comput. Assist. Interv., 5th, Part II, Tokyo*, pp. 525–32. Berlin/Heidelberg: Springer-Verlag
31. Ou Y, Sotiras A, Paragios N, Davatzikos C. 2010. DRAMMS: deformable registration via attribute matching and mutual-saliency weighting. *Med. Image Anal.* In press
32. Lee D, Hofmann M, Steinke F, Altun Y, Cahill ND, Scholkopf B. 2009. Learning similarity measure for multi-modal 3D image registration. *Proc. Comput. Vis. Pattern Recognit., June 20–25, Miami*, pp. 186–93. Piscataway, NJ: IEEE
33. Bronstein M, Bronstein A, Michel F, Paragios N. 2010. Data fusion through cross-modality metric learning using similarity-sensitive hashing. *Proc. Comput. Vis. Pattern Recognit., June 13–18, San Francisco*, pp. 3594–601. Piscataway, NJ: IEEE
34. Jeyakumar V, Rubinov A, eds. 2005. *Continuous Optimization: Current Trends and Modern Applications*. New York: Springer
35. Papadimitriou CH, Steiglitz K. 1998. *Combinatorial Optimization: Algorithms and Complexity*. Mineola, NY: Dover
36. Li SZ. 2009. *Markov Random Field Modeling in Image Analysis*. New York: Springer. 3rd ed.
37. Lee JD, Huang CH, Wang ST, Lin CW, Lee ST. 2010. Fast-MICP for frameless image-guided surgery. *Med. Phys.* 37(9):4551–59
38. Chui H, Win L, Schultz R, Duncan JS, Rangarajan A. 2003. A unified non-rigid feature registration method for brain mapping. *Med. Image Anal.* 7:113–30
39. Maurer CR, Maciunas RJ, Fitzpatrick JM. 1998. Registration of head CT images to physical space using a weighted combination of points and surfaces. *IEEE Trans. Med. Imaging* 17(5):753–61
40. Papademetris X, Sinusas AJ, Dione DP, Constable RT, Duncan JS. 2002. Estimation of 3-D left ventricular deformation from medical images using biomechanical models. *IEEE Trans. Med. Imaging* 21(7):786–800
41. Makela T, Clarysse P, Sipila O, Pauna N, Pham QC, et al. 2002. A review of cardiac image registration methods. *IEEE Trans. Med. Imaging* 21(9):1011–21
42. Joshi S, Davis B, Jornier M, Gerig G. 2004. Unbiased diffeomorphic atlas construction for computational anatomy. *NeuroImage* 23(1):S151–60
43. Lorenzen P, Prastawa M, Davis B, Gerig G, Bullitt E, Joshi S. 2006. Multi-modal image set registration and atlas formation. *Med. Image Anal.* 10(3):440–51
44. Vercauteren T, Ayache N, Savoire N, Malandain G, Perchant A. 2008. Processing of in vivo fibered confocal microscopy video sequences. In *Microscopic Image Analysis for Life Science Applications*, ed. J Rittscher, R Machiraju, STC Wong, pp. 441–63. Norwood, MA: Artech
45. Rogelj P, Kovacic S, Gee JC. 2003. Point similarity measures for non-rigid registration of multi-modal data. *Comput. Vis. Image Underst.* 92(1):112–40
46. Loeckx D, Maes F, Vandermeulen D, Suetens P. 2004. Nonrigid image registration using free-form deformations with a local rigidity constraint. *Proc. Med. Image Comput. Comput. Assist. Interv., 7th, Part I, Saint-Malo, Fr.*, pp. 639–46. Berlin/Heidelberg: Springer-Verlag
47. Rohlfing T, Maurer CR, Bluemke DA, Jacobs MA. 2003. Volume-preserving nonrigid registration of MR breast images using free-form deformation with an incompressibility constraint. *IEEE Trans. Med. Imaging* 22(6):730–41
48. Thirion J. 1998. Image matching as a diffusion process: an analogy with Maxwell's demons. *Med. Image Anal.* 2(3):243–60
49. Hermosillo G, Chefd'Hotel C, Faugeras O. 2002. Variational methods for multimodal image matching. *Int. J. Comput. Vis.* 50(3):329–43
50. Klein S, Staring M, Pluim JPW. 2007. Evaluation of optimization methods for nonrigid medical image registration using mutual information and B-splines. *IEEE Trans. Image Process.* 16(12):2879–90
51. Vercauteren T, Pennec X, Perchant A, Ayache N. 2009. Diffeomorphic demons: efficient non-parametric image registration. *NeuroImage* 45(1):S61–72
52. Godley A, Ahunbay E, Peng C, Li XA. 2009. Automated registration of large deformations for adaptive radiation therapy of prostate cancer. *Med. Phys.* 36(4):1433–41

53. Heimann T, Meinzer HP. 2009. Statistical shape models for 3D medical image segmentation: a review. *Med. Image Anal.* 13(4):543–63
54. Johnson HJ, Christensen GE. 2002. Consistent landmark and intensity-based image registration. *IEEE Trans. Med. Imaging* 21(5):450–61
55. Cachier P, Mangin JF, Pennec X, Riviére D, Papadopoulos-Orfanos D, Règis J. 2001. Multisubject non-rigid registration of brain MRI using intensity and geometric features. *Proc. Med. Image Comput. Comput. Assist. Interv., 4th, Utrecht, Neth.*, pp. 734–42. Berlin/Heidelberg: Springer-Verlag
56. Biesdorf A, Wörz S, Kaiser HJ, Stippich C, Rohr K. 2009. Hybrid spline-based multimodal registration using local measures for joint entropy and mutual information. *Proc. Med. Image Comput. Comput. Assist. Interv., 12th, Part I, London*, pp. 607–15. Berlin/Heidelberg: Springer-Verlag
57. Papademetris X, Jakowski AP, Schultz RT, Staib LH, Duncan JS. 2004. Integrated intensity and point-feature non-rigid registration. *Proc. Med. Image Comput. Comput. Assist. Interv., 7th, Part I, Saint-Malo, Fr.*, pp. 763–70. Berlin/Heidelberg: Springer-Verlag
58. Hellier P, Barillot C. 2003. Coupling dense and landmark-based approaches for non-rigid registration. *IEEE Trans. Med. Imaging* 22(2):217–27
59. Sotiras A, Ou Y, Glocker B, Davatzikos C, Paragios N. 2010. Simultaneous geometric–iconic registration. *Proc. Med. Image Comput. Comput. Assist. Interv., 13th, Part II, Beijing*, pp. 676–83. Berlin/Heidelberg: Springer-Verlag
60. Sederberg TW, Parry SR. 1986. Free-form deformation of solid geometric models. *Proc. Annu. Conf. Comput. Graph. Interact. Tech. (SIGGRAPH), 13th, Dallas*, pp. 151–60. New York: Assoc. Comput. Mach.
61. Glocker B, Komodakis N, Tziritas G, Navab N, Paragios N. 2008. Dense image registration through MRFs and efficient linear programming. *Med. Image Anal.* 12(6):731–41
62. Besag J. 1986. On the statistical analysis of dirty pictures. *J. R. Stat. Soc. Ser. B* 48:259–302
63. Chou PBL. 1988. *The Theory and Practice of Bayesian Image Labeling*. New York: Univ. Rochester
64. Chellappa R, Jain A, eds. 1993. *Markov Random Fields: Theory and Application*. San Diego, CA: Academic
65. Kirkpatrick S, Gelatt CD, Vecchi MP. 1983. Optimization by simulated annealing. *Science* 220:671–80
66. Greig DM, Porteous BT, Seheult AJ. 1989. Exact minimum a posteriori estimation for binary images. *J. R. Stat. Soc. Ser. B* 51(2):271–79
67. Pearl J. 1988. *Probabilistic Reasoning in Intelligent Systems: Networks of Plausible Inference*. San Francisco: Morgan Kaufmann
68. Komodakis N, Tziritas G. 2007. Approximate labeling via graph cuts based on linear programming. *IEEE Trans. Pattern Anal. Mach. Intell.* 29(8):1436–53
69. Ford LR Jr, Fulkerson DR. 1962. *Flows in Networks*. Princeton, NJ: Princeton Univ. Press
70. Goldberg AV, Tarjan RE. 1988. A new approach to the maximum-flow problem. *J. Assoc. Comput. Mach.* 35(4):921–40
71. Boykov Y, Veksler O, Zabih R. 2001. Fast approximate energy minimization via graph cuts. *IEEE Trans. Pattern Anal. Mach. Intell.* 23(11):1222–39
72. Woodford O, Torr P, Reid I, Fitzgibbon A. 2009. Global stereo reconstruction under second-order smoothness priors. *IEEE Trans. Pattern Anal. Mach. Intell.* 31(12):2115–28
73. Kohli P, Torr PHS. 2007. Dynamic graph cuts for efficient inference in Markov random fields. *IEEE Trans. Pattern Anal. Mach. Intell.* 29(12):2079–88
74. Kolmogorov V, Zabih R. 2004. What energy functions can be minimized via graph cuts? *IEEE Trans. Pattern Anal. Mach. Intell.* 26(2):147–59
75. Frey BJ, MacKay DJC. 1997. A revolution: belief propagation in graphs with cycles. In *Advances in Neural Information Processing Systems 10*, ed. MI Jordan, MJ Kearns, SA Solla, pp. 479–85. Cambridge, MA: MIT Press
76. Felzenszwalb P, Huttenlocher D. 2006. Efficient belief propagation for early vision. *Int. J. Comput. Vis.* 70:41–54
77. Kolmogorov V. 2006. Convergent tree-reweighted message passing for energy minimization. *IEEE Trans. Pattern Anal. Mach. Intell.* 28(10):1568–83
78. Komodakis N, Paragios N, Tzirita G. 2011. MRF energy minimization and beyond via dual decomposition. *IEEE Trans. Pattern Anal. Mach. Intell.* 33(3):531–52

79. Komodakis N, Tziritas G, Paragios N. 2008. Performance versus computational efficiency for optimizing single and dynamic MRFs: setting the state of the art with primal dual strategies. *Comput. Vis. Image Underst.* 112(1):14–29
80. Komodakis N, Paragios N. 2008. Beyond loose LP-relaxations: optimizing MRFs by repairing cycles. *Proc. Eur. Conf. Comput. Vis., 10th, Part III, Marseille, Fr.*, pp. 806–20. Berlin/Heidelberg: Springer-Verlag
81. Glocker B, Komodakis N, Paragios N, Tziritas G, Navab N. 2007. Inter- and intra-modal deformable registration: continuous deformations meet efficient optimal linear programming. *Inf. Process. Med. Imaging* 20:408–20
82. Glocker B, Komodakis N, Paragios N, Glaser C, Tziritas G, Navab N. 2007. Primal/dual linear programming and statistical atlases for cartilage segmentation. *Proc. Med. Image Comput. Comput. Assist. Interv., 10th, Part II, Brisbane, Aust.*, pp. 536–43. Berlin/Heidelberg: Springer-Verlag
83. Wachinger C, Glocker B, Zeltner J, Paragios N, Komodakis N, et al. 2008. Deformable mosaicing for whole-body MRI. *Proc. Med. Image Comput. Comput. Assist. Interv., 11th, Part II, New York*, pp. 113–21. Berlin/Heidelberg: Springer-Verlag
84. Sotiras A, Neji R, Deux J-F, Komodakis N, Fleury G, Paragios N. 2010. A kernel-based graphical model for diffusion tensor registration. *Proc. IEEE Int. Symp. Biomed. Imaging, Apr. 14–17, Rotterdam*, pp. 524–27. Piscataway, NJ: IEEE
85. Sotiras A, Komodakis M, Glocker B, Deux JF, Paragios N. 2009. Graphical models and deformable diffeomorphic population registration using global and local metrics. *Proc. Med. Image Comput. Comput. Assist. Interv., 12th, Part I, London*, pp. 672–79. Berlin/Heidelberg: Springer-Verlag
86. Rueckert D, Aljabar P, Heckemann R, Hajnal J, Hammers A. 2006. Diffeomorphic registration using B-splines. *Proc. Med. Image Comput. Comput. Assist. Interv., 9th, Part II, Copenhagen*, pp. 702–9. Berlin/Heidelberg: Springer-Verlag
87. Vandemeulebroucke J, Sarrut D, Clarysse P. 2007. The POPI-model, a point-validated pixel-based breathing thorax model. *Proc. Int. Conf. Use Comput. Radiat. Ther., 15th, Toronto*, pp. 1–8. Oakville, Can.: Novel Digital
88. Sarrut D, Boldea V, Miguet S, Ginestet C. 2006. Simulation of four-dimensional CT images from deformable registration between inhale and exhale breath-hold CT scans. *Med. Phys.* 33(3):605–17
89. Delhay B, Clarysse P, Pera C, Magnin IE. 2006. A spatio-temporal deformation model for dense motion estimation in periodic cardiac image sequences. *Proc. Med. Image Comput. Comput. Assist. Interv. Workshop, 9th, Copenhagen*, pp. 87–90. Berlin/Heidelberg: Springer-Verlag
90. Baker S, Scharstein D, Lewis J, Roth S, Black M, Szeliski R. 2010. A database and evaluation methodology for optical flow. *Int. J. Comput. Vis.* 92:1–31
91. Glocker B, Paragios N, Komodakis N, Tziritas G, Navab N. 2008. Optical flow estimation with uncertainties through dynamic MRFs. *Proc. Comput. Vis. Pattern Recognit., June 23–28, Anchorage, Alsk.* pp. 1–8. Piscataway, NJ: IEEE
92. Glocker B, Komodakis N, Navab N, Tziritas G, Paragios N. 2009. Dense registration with deformation priors. *Inf. Process. Med. Imaging* 21:540–51
93. Kwon D, Lee K, Yun I, Lee S. 2008. Nonrigid image registration using dynamic higher-order MRF model. *Proc. Eur. Conf. Comput. Vis., 10th, Part I, Marseille, Fr.*, pp. 373–86. Berlin/Heidelberg: Springer-Verlag

Annual Review of Biomedical Engineering
Volume 13, 2011

Contents

Indexes

Errata

An online log of corrections to *Annual Review of Biomedical Engineering* articles may be found at http://bioeng.annualreviews.org/